symmetry

MDPI

Article

Thermal Conductivity Modeling of Nanofluids Contain MgO Particles by Employing Different Approaches

Na Wang [1], Akbar Maleki [2], Mohammad Alhuyi Nazari [3], Iskander Tlili [4,5,*] and Mostafa Safdari Shadloo [6]

1 Department of Anesthesiology, the First Hospital of Jilin University, Changchun 130021, China; lilyly12345@163.com
2 Faculty of Mechanical Engineering, Shahrood University of Technology, Shahrood 3619995161, Iran; A_maleki@shahrood.ut.ac.ir
3 Department of Renewable Energies, Faculty of New Science & Technologies, University of Tehran, Tehran 5441656498, Iran; Nazari.mohammad.a@ut.ac.ir
4 Department for Management of Science and Technology Development, Ton Duc Thang University, Ho Chi Minh City 758307, Vietnam
5 Faculty of Applied Sciences, Ton Duc Thang University, Ho Chi Minh City 758307, Vietnam
6 CORIA-UMR 6614, Normandie University, CNRS-University & INSA, 76000 Rouen, France; msshadloo@coria.fr
* Correspondence: iskander.tlili@tdtu.edu.vn

Received: 26 December 2019; Accepted: 16 January 2020; Published: 1 February 2020

Abstract: The existence of solid-phase nanoparticles remarkably improves the thermal conductivity of the fluids. The enhancement in this property of the nanofluids is affected by different items such as the solid-phase volume fraction and dimensions, temperature, etc. In the current paper, three different mathematical models, including polynomial correlation, Multivariate Adaptive Regression Spline (MARS), and Group Method of Data Handling (GMDH), are applied to forecast the thermal conductivity of nanofluids containing MgO particles. The inputs of the model are the base fluid thermal conductivity, volume concentration, and average dimension of solid-phase, and nanofluids' temperature. Comparing the proposed models revealed higher confidence of GMDH in estimating the thermal conductivity, which is attributed to its complicated structure and more appropriate consideration of the input's interaction. The values of R-squared for the correlation, MARS, and GMDH are 0.9949, 0.9952, and 0.9991, respectively. In addition, based on the sensitivity analysis, the effect of thermal conductivity of the base fluid on the overall thermal conductivity of nanofluids is more remarkable compared with the other inputs such as volume fraction, temperature, and dimensions of the particles which are used as the inputs of the models.

Keywords: nanofluid; thermal conductivity; MgO nanoparticles; GMDH; MARS

1. Introduction

Thermal Conductivity (TC) of fluids influence their performance as heat transfer fluid in thermal mediums [1–3]. Adding nanodimensional solid structures into the pure conventional heat transfer fluids such as water, Ethylene Glycol (EG), and oils can remarkably enhance their TC [4–8]. For instance, Shameil et al. [9] found that the TC of DWCNT/ethylene glycol in 0.6% volume fraction of solid phase and 52 °C is enhanced by 24.9% compared with the pure base fluid. Guo et al. [10] measured TC of SiO_2/water and SiO_2/EG and observed that in 1% vol concentration, the TC of water- and EG-based nanofluids increased by 3.4% and 9.6%, respectively. In another experimental research study [11],

the effect on Al_2O_3 nanoparticle dispersion in water and EG at different temperatures on the TC was investigated, and an increase in TC was observed in the case of solid particle dispersion in EG. Based on the literature review, an increment in the TC was dependent on the type of the base fluid, concentration, and temperature [12–15]. For instance, at 10 °C, the highest increases in the TC of water- and EG-based nanofluids were 13% and 20%, while these values increased to 15% and 25% at 70 °C, respectively. A higher increment in increased temperatures can be due to the Brownian motions of the solid particles [16]. In addition to the single type particles, hybrid nanostructures have been used in pure fluids for TC improvement. According to a study conducted by Hemmat Esfe et al. [17], adding $SiO_2 - DWCNT$ in 1.71%, volumetric concentration into EG resulted in up to a 38% increment in the TC.

Improved thermophysical feature of the fluids containing nanostructures makes them as favorable candidates for heat transfer fluid in thermal systems such as heat pipes, solar collectors, heat exchangers, etc. [18–24]. Elsayed et al. [25], carried out a numerical study on heat transfer of turbulent flow inside a helically coiled tube and concluded that using Al_2O_3/water instead of water led to 60% increase in heat transfer coefficient. MgO is one of the most attractive materials for preparing nanofluids due to its ability in providing more appropriate thermal features compared with other metal oxide particles [26,27]. Nanofluids containing MgO particles are widely utilized in different systems in order to achieve improved efficiency and heat transfer. Verma et al. [28] used MgO/water in a flat plate solar collector and observed that employing the nanofluid in 0.75% vol concentration instead of water resulted in up to 9.34% and 32.23% increases in the thermal and energetic efficiencies, respectively. Menlik et al. [29] applied MgO/water nanofluid in a heat pipe and observed that employing the nanofluid led to a 26% enhancement in the effectiveness of nanofluid-charged heat pipe.

Several methods and approaches are suggested for estimating the thermophysical properties of the nanofluids [30–33]. Artificial Neural Networks (ANNs), Support Vector Machines (SVMs), and correlation obtained by curve fitting are among the most applicable ones used in recent years [34–37]. Wu et al. [38] utilized curve fitting for the TC modeling of ZnO-multi walled carbon nano tube (MWCNT)/engine oil nanofluid by using the solid phase fraction and temperature as the inputs and observed that the proposed correlation was able to predict the TC of the nanofluid with maximum deviation lower than 1%. In another research, Hemmat et al. [39] proposed a correlation-based model on similar inputs for forecasting the TC of CuO/EG-water nanofluid. The value of R-squared for their proposed correlation was 0.9850. In the majority of the proposed models for TC forecasting [39], just temperature and volume fraction are considered for modeling, while adding the dimensions of the solid-phase result in finding more comprehensive models with applicability for different case studies [40,41]; in this regard, Ahmadi et al. [42] applied different artificial neural network (ANN)-based methods such as multilayer perceptron, Adaptive Neuro-Fuzzy Inference System (ANFIS) and Radial Basis Function (RBF) for modeling the TC of TiO_2/water nanofluid. The closeness of the estimated values by the models and the experimental values demonstrated the confident performance of ANNs for modeling.

The present paper is focused on the TC modeling of the nanofluids containing MgO particles for different values of temperature, size, volume fraction, and base fluids' TC. In this regard, different approaches such as polynomial correlation, multivariate adaptive regression spline (MARS), and group method of data handling (GMDH) ANN are employed. Finally, the outputs of the models are compared with the actual values of nanofluids' TC, obtained in different experimental studies, to evaluate the confidence of the models based on different statistical criteria. Moreover, the relative importance of the inputs is determined and explained.

2. Methodology

In the present article, three methods are employed for estimating the TC of nanofluids containing MgO particles. In the first stage, a polynomial of degree two is used for the regression. The main advantages of using polynomials for proposing predictive models are their ease for utilization and simplicity of the structure. Afterward, MARS and GMDH ANN are employed for forecasting the TC

of the nanofluids. MARS approach is a nonparametric type of regression method which utilizes some basis functions for modeling complex input-output relationships. This model can be expressed as:

$$y = f(X) + e \tag{1}$$

where X refers to independent input variables, y is the output, f is the weighted basis function which is dependent on the inputs, and e denotes the error vector. In the MARS technique, piecewise linear regression functions are used in order to fit data and find nonlinear relationships between the inputs and the output. The relationships are found by employing piecewise polynomials and sets of coefficients [43]. This model is achieved by fitting the basis functions into distinct ranges of input variables. Put et al. [44] investigated the MARS global technique. It is defined as follows (Equation (2)):

$$\hat{y} = \beta_0 + \sum_{m=1}^{M} \beta_m \, h_m(X) \tag{2}$$

$\hat{y}$ and β_0 in Equation (2) are the prognosticated response and the coefficient of the basis function, respectively. The mth basic function is represented as $h_m(X)$. It can have the form of either a single polynomial or a combination of more polynomial functions. Furthermore, β_m is a coefficient relating to the mth basis function. The number of basis functions that the MARS algorithm takes into consideration is counted by M.

In the MARS technique, there are three main stages. The first one is known as the constructive step. It adds the basis functions using a stepwise forward method. In addition, two substantial parameters (i.e., locations of nodes and the predictor) are being selected in this stage of the MARS technique. They have considerable effect on the accuracy of the results.

In the first step, interactions are given in order to study their relevance with the model fit refinement.

Secondly, with the aim of enhancing the prediction, the goal is to eliminate the superfluous basis functions. This is done through a backward stepwise approach. In the MARS technique, the Generalized Cross-Validation (GCV) is used as a criterion in order to specify the most effective model among many currently available models. A high value of GCV makes a smaller model, and a lower quantity for GCV suggests a bigger produced model. Equation (5) shows the GCV criterion [43,45]:

$$GCV = \frac{1}{N} \frac{\sum_{i=1}^{N} \left(y_i - \hat{f}(X_i)\right)^2}{\left[1 - \frac{\widetilde{C}(M)}{N}\right]^2} \tag{3}$$

The term $\left[1 - \frac{\widetilde{C}(M)}{N}\right]^2$ in Equation (3) is a complexity function. Furthermore, $\widetilde{C}(M)$ is defined as $C(M) + dM$. Here, d is the cost of each of the basis functions. It can be decided based on the user's requirements. This parameter specifies the soothing of the approach. $C(M)$ is considered as the value of the elements that should be fit. The parameter d in Equation (3) sets the number of the basis functions that can be eliminated.

It can be inferred that as the cost increases, more basis functions are eradicated. Ultimately, in the third stage, the optimized MARS technique is determined. This is done based on the assessment of the characteristics of the proposed fit models. More details about this method can be found in Refs [43,45]. GCV function is utilized in order to figure out the significance score of the input variables. The input variables' relative importance indicates an increment in the quantity of the GCV as the applied basis function having specific variables are dropped and the other basis functions refit to the target, in the genuine form, by applying ordinary least square (OLS) regression. The details of this approach are represented in [43,46].

ANNs are applicable in different fields of study for predicting the behavior of the systems and their modeling [47–51]. The third approach used for forecasting the TC of the nanofluids with MgO

particles is GMDH. This approach has some advantages in comparison with other conventional ANNs, such as no requirement for precondition definitions, including the number of layers and neurons, due to its self-regulating property. In this approach, the repetitive procedure is performed in order to accurate calculation of the variable considered as the target (P). The schematic of the procedure applied in GMDH is shown in Figure 1. In the process of modeling by applying GMDH, polynomials of degree two are utilized in the first step and its complicity increases by an increment in the number of layers. An increase in the number of layers depends on the required effectiveness of the model. In this procedure, in the case of having n inputs and an output, Kolmogorov–Gabor polynomial is generated to form the network.

$$P = \alpha_0 + \sum_{i=1}^{n} \omega_i X_i + \sum_{i=1}^{n}\sum_{j=1}^{n} \omega_{ij} X_i X_j + \sum_{i=1}^{n}\sum_{j=1}^{n}\sum_{k=1}^{n} \omega_{ijk} X_i X_j X_k + \cdots \quad (4)$$

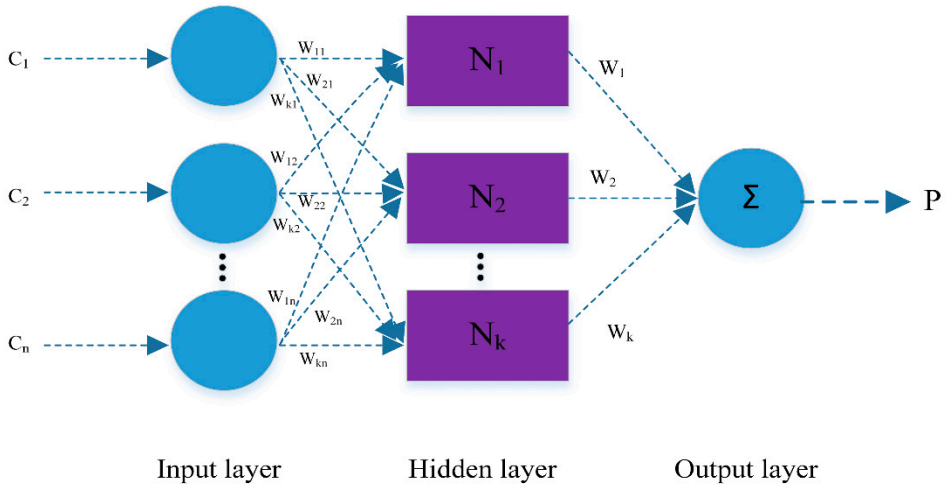

Figure 1. Structure of GMDH model [52].

In this equation, X refers to the vector used as input, ω is the weight vector, and P is the forecasted output. The output of the model is determined by utilizing the least square approach by determining the minimum mean square error value. In the case of using Xi and Xj as the inputs, the overall obtained polynomial can be defined as:

$$P = \alpha_0 + \alpha_1 X_i + \alpha_2 X_j + \alpha_3 X_i X_j + \alpha_4 X_i^2 + \alpha_5 X_j^2 \quad (5)$$

This approach is explained with more details in several references [53–55].

3. Results and Discussion

Since the aim of the present study is proposing a model with applicability for different base fluids in various temperature, volume fraction, and dimensions of particles, several references were used for data extraction [27,56–60]. The base fluids of the considered case studies were engine oil, water, EG, and mixtures of EG-water. In order to quantitatively consider the impact of the base fluid in the model, their TC at 25 °C was added to the volume fraction, size, and temperature, which have been used in previous studies. The ranges of temperature and volume fraction of the extracted data were 10–55 °C and 0.1–7.2%, respectively. Nanoparticles with average diameters in the range of 10 and 60 mm were used in the case studies.

As was previously noted, a polynomial of degree two is used for the modeling. The structure of the polynomial is designed as:

$$TC = a * x_1 + b * x_2 + c * x_3 + d * x_4 + e * x_1^2 + f * x_2^2 + g * x_3^2 + h * x_4^2 + i * x_1 * x_2 + j * x_1 * x_3 + k * x_1 * x_4 + l * x_2 * x_3 + m * x_2 * x_4 + n * x_3 * x_4 + o \quad (6)$$

where x_1, x_2, x_3, and x_4 are the TC of the base fluid, size of the particles, volume fraction, and temperature, respectively. The obtained values of the abovementioned correlation are represented in Table 1.

Table 1. Determined coefficients of the polynomial.

a	b	c	d	e	f	g	h
0.960011	0.002045	0.006512	−0.00081	−0.20459	−0.000024	0.000235	−0.00001
i	j	k	l	m	n	o	
−0.00076	0.051041	0.007562	−0.00014	0	0.00006	−0.01792	

In Figure 2, the obtained values of the TC are compared with the actual quantities measured in the experimental researches. In this case, the R-squared value is 0.9949. In addition to R-squared, the relative deviation of the model is determined to indicate the confidence of the model. The corresponding relative deviation for each data index is shown in Figure 3. In this case, the maximum relative deviation is about 12.2%.

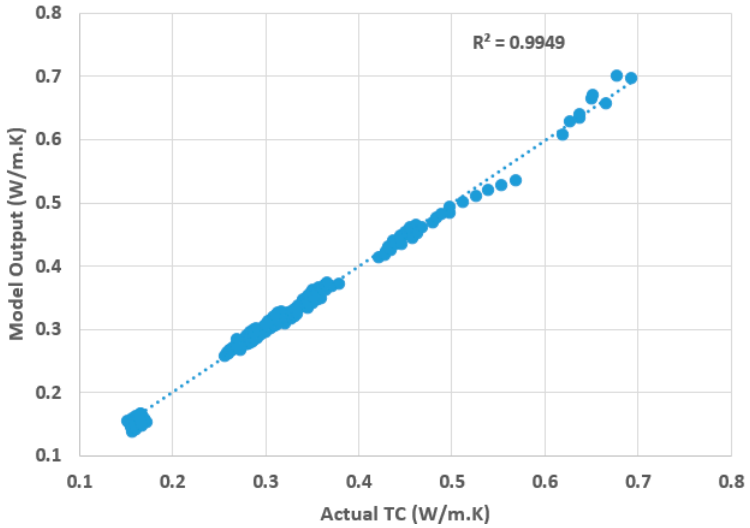

Figure 2. Comparison between the values obtained by the correlation and experimental data.

In the second step, the MARS method is used for modeling the TC of the nanofluids. The determined relationships between the inputs and the TC by employing the MARS approach is as below:

$$\begin{aligned} TC = 0.278929 \quad & +1.24943 * BF1 - 0.955071 * BF2 + 0.0210546 * BF3 \\ & -0.0804188 * BF4 - 0.441445 * BF5 - 0.00479838 * BF7 \\ & -0.00058189 * BF8 - 0.000408513 * BF9 - 0.00911003 * BF10 \\ & +0.00230784 * BF12 \end{aligned} \quad (7)$$

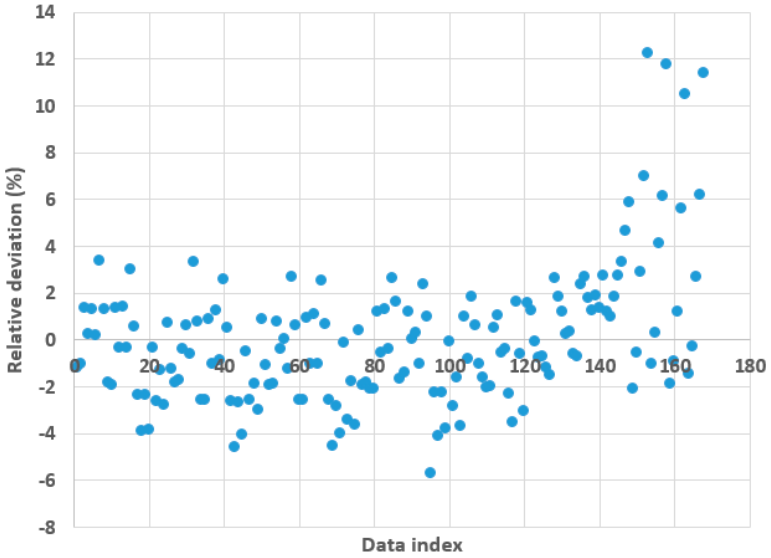

Figure 3. Relative deviation vs. data index for the proposed correlation.

The basis functions used in the abovementioned equations are shown in Table 2.

Table 2. Determined basis functions of the MARS method.

Basis Functions	***BF*1**	***BF*2**	***BF*3**	***BF*4**	***BF*5**
Relationship	$\max(0, x_1 - 0.251)$	$\max(0, 0.251 - x_1)$	$\max(0, x_3 - 0.25)$	$\max(0, 0.25 - x_3)$	$\max(0, x_1 - 0.408)$
Basis Functions	***BF*7**	***BF*8**	***BF*9**	***BF*10**	***BF*12**
Relationship	$\max(0, x_4 - 50)$	$\max(0, 50 - x_4)$	$\max(0, x_2 - 10)$	$\max(0, x_3 - 4)$	$\max(0, x_4 - 45)$

In Figure 4, the forecasted values of TC are compared with the corresponded quantities measured in the experimental researches. In this case, the R-squared is equal to 0.9952. The higher value of the R-squared in the case of using the MARS method compared with the proposed correlation reveals the higher confidence of the model. The improved accuracy of the model by employing the MARS approach can be attributed to its more complex structure, which results in better consideration of input variables interactions. In addition to R-squared, these methods can be compared on the basis of relative deviation. As shown in Figure 5, the maximum value of relative deviation in the case of applying MARS for TC modeling is 13.76%; however, in most cases, its values are lower compared with the proposed correlation.

Finally, a model is proposed for the TC of the nanofluids by using GMDH ANN. The obtained relationship for the inputs and the output of the model is:

$$TC = -8.7104 * 10^{-5} + N153 * 0.0556369 + N2 * 0.944621 \quad (8)$$

The procedure of determining the coefficients are represented in Appendix A. In this case, the R-squared is 0.9991, which is higher compared with the determined values of the previous models. In Figure 6, the TCs obtained with the model and actual values are compared. In addition, comparing the values of relative deviation demonstrates more confidence in the prediction in the case of using GMDH in comparison with using the MARS method and mathematical correlation. As illustrated in Figure 7, the maximum absolute value of the relative deviation is approximately 3.18% when GMDH was applied for modeling.

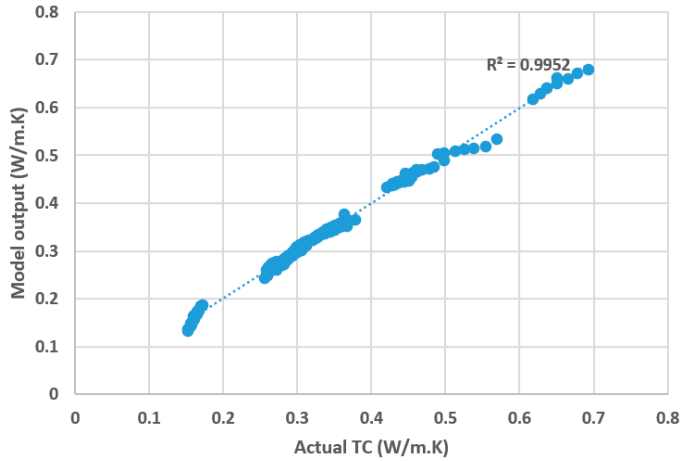

Figure 4. Comparison between the values obtained by the MARS method and the experimental data.

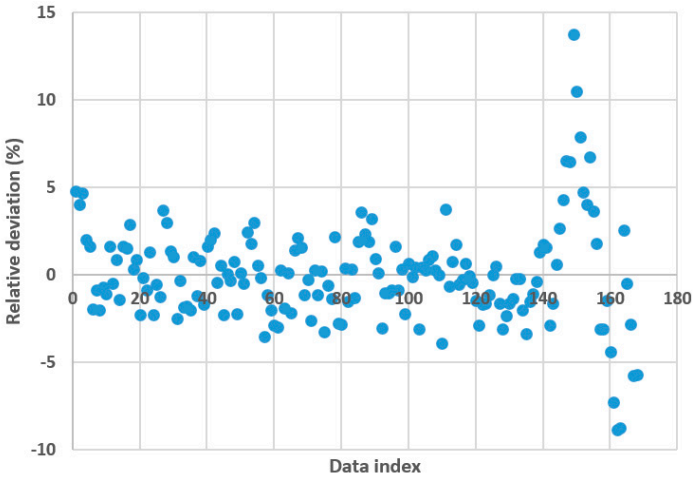

Figure 5. Relative deviation vs. data index for the MARS model.

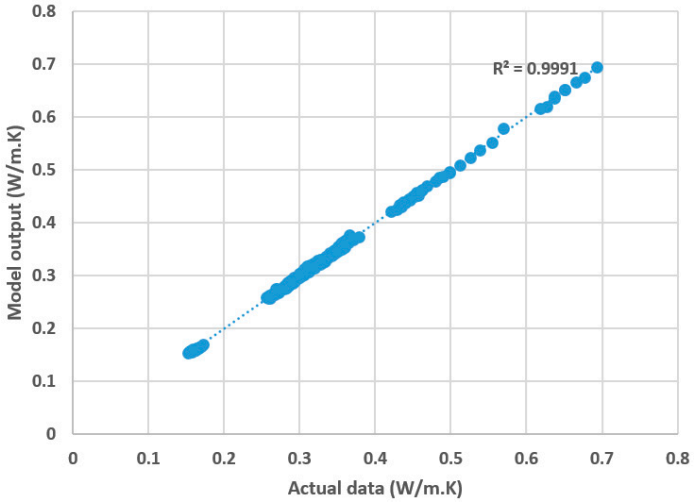

Figure 6. Comparison between the values obtained by the GMDH method and the experimental data.

Figure 7. Relative deviation v.s.data index for the GMDH model.

In order to havema deeper insight into the accuracy of the models in predicting the data, using average absolute relative deviation can be more useful, which provides the possibility of comparing the accuracy of the models for the total data. As shown in Figure 8, the average absolute relative deviations of the correlation, MARS, and GMDH in modeling, are approximately 3.22%, 2.03%, and 0.90%, respectively.

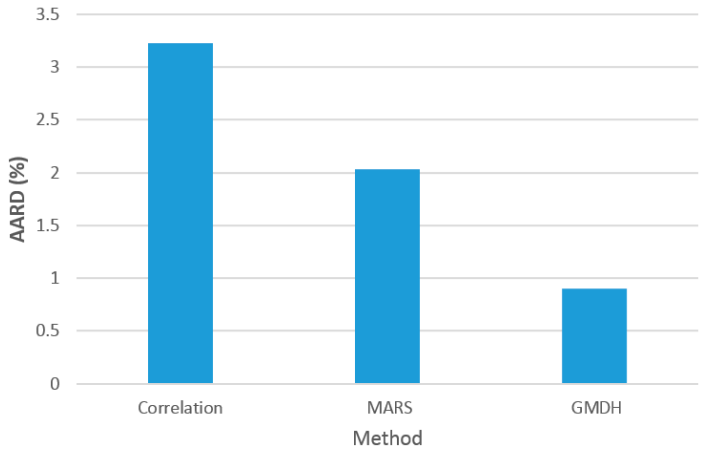

Figure 8. Average relative deviation of each model.

The relative importance of the inputs provides useful information about the role of each input on the outputs of the model. Based on the sensitivity analysis, the TC of the base fluid has the most crucial role in the value of the nanofluids' TC. In Figure 9, the importance of variables is shown.

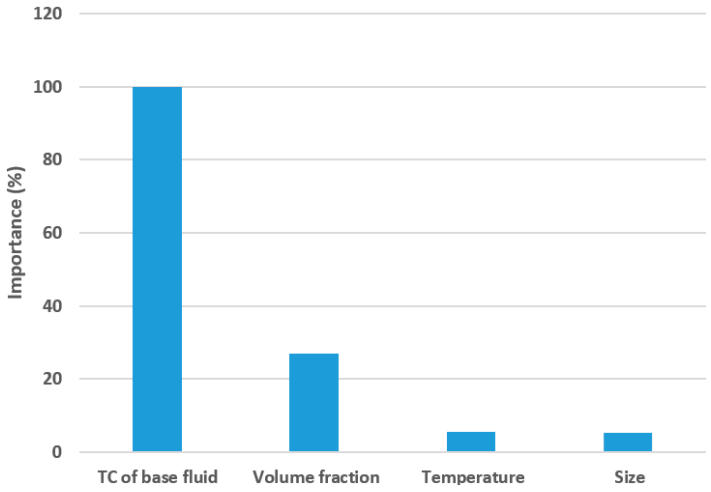

Figure 9. Importance of variables.

4. Conclusions

In this paper, three methods, including a mathematical correlation, MARS, and GMDH ANN were applied to forecast the thermal conductivity of nanofluids containing MgO nanoparticles. The inputs of the proposed models were thermal conductivity of the base fluid, volume fraction, and dimensions of CuO particles and temperature. Models comparison revealed that employing GMDH resulted in the highest confidence. The average absolute relative deviations of the models in the cases of employing correlation, MARS, and GMDH methods were approximately 3.22%, 2.03%, and 0.90%, respectively. In addition, based on the performed sensitivity analysis, thermal conductivity of the base fluid had the most noticeable impact on the thermal conductivity of the nanofluids. The R-squared of the proposed models by using the correlation, MARS and GMDH approaches, were 0.9949, 0.9952, and 0.9991, respectively. According to these determined values, all of the models are reliable and appropriate for forecasting the thermal conductivity of the nanofluids with dispersed MgO particles.

Author Contributions: The N.W. and M.A.N. conducted modeling and writing, revising the article is carried out by the M.S.S. A.M. and I.T. supervised the research and edited it. All authors have read and agreed to the published version of the manuscript.

Funding: This research received no external funding.

Conflicts of Interest: The authors declare no conflicts of interest.

Appendix A

$$TC = -8.7104 * 10^{-5} + N153 * 0.0556369 + N2 * 0.944621$$

$$N2 = 6.33392 * 10^{-5} - N73 * 0.111613 + N3 * 1.11143$$

$$N3 = 0.00138188 + N59 * N5 * 74.1406 - N59^2 * 37.0879 + N5 * 0.995333 - N5^2 * 37.0464$$

$$N5 = -0.00147952 + N31 * 0.241927 - N31 * N6 * 73.7483 + N31^2 * 36.7664 + N6 * 0.763533 + N6^2 * 36.9748$$

$$N6 = 0.0002285 - N114 * 0.460449 + N14 * 1.45977$$

$$N14 = 0.000105035 + N18 * 0.643206 + N18 * N25 * 28.8074 - N18^2 * 14.4924 + N25 * 0.357674 - N25^2 * 14.3163$$

$$N25 = 0.00218015 + N332 * N54 * 3.67579 - N332^2 * 2.02706 + N54 * 0.997428 - N54^2 * 1.65177$$

$$N54 = -0.0408802 - N355 * N74 * 0.693239 + N355^2 * 0.46511 + N74 * 1.17673 + N74^2 * 0.0616494$$

$$N355 = 0.371309 + N360 * 0.71474 - N364 * 1.58917 + N364^2 * 2.24705$$

$$N364 = 3.27276 + x_4 * 0.0100847 - {x_4}^2 * 0.000152815 - N370 * 17.6064 + N370^2 * 24.9277$$

$$N332 = -0.370344 + N342 * 0.804179 + N342 * N368 * 1.20998 - N342^2 * 0.315614 + N368 * 2.05621 - N368^2 * 3.08519$$

$$N368 = 2.7631 - N371 * 15.8134 + N371^2 * 25.3292$$

$$N342 = -0.00477946 + x_2 * 0.000167309 - x_2 * N343 * 0.000270589 - {x_2}^2 * 9.30425 * 10^{-7} + N343 * 1.00992$$

$$N18 = -0.00710574 - N196 * 1.02626 - N196 * N41 * 1.99319 + N196^2 * 1.94146 + N41 * 2.06698$$

$$N41 = 0.00157139 + N304 * N69 * 5.7359 - N304^2 * 3.01962 + N69 * 1.00069 - N69^2 * 2.71984$$

$$N69 = 0.000476153 + N137 * 0.994991 + N137 * N187 * 0.832487 - N137^2 * 0.822307$$

$$N137 = 0.00611404 + x_1 * 1.06531 - x_1 * N175 * 3.09998 + N175^2 * 2.85239$$

$$N175 = 0.0749914 - x_4 * 0.00157427 + x_4 * N227 * 0.00678305 + N227 * 0.598162 + N227^2 * 0.279983$$

$$N304 = -0.386619 + N337 * 0.721253 + N337 * N358 * 1.48285 - N337^2 * 0.277372 + N358 * 2.17904 - N358^2 * 3.35703$$

$$N358 = 2.16103 - N370 * 11.3861 - N370 * N371 * 17.9324 + N370^2 * 25.0097 + N371^2 * 10.3783$$

$$N337 = 0.0210866 - x_2 * 0.000486486 + {x_2}^2 * 3.01016 * 10^{-7} + N348 * 0.993111$$

$$N196 = 0.0776005 - x_4 * 0.00165255 + x_4 * N243 * 0.00696503 + N243 * 0.591801 + N243^2 * 0.28152$$

$$N243 = 0.23064 + N249 * 0.98187 + N249^2 * 0.0104777 - N369 * 1.37367 + N369^2 * 2.06441$$

$$N114 = 0.0141143 + x_1 * 0.584343 - x_1 * N144 * 1.99686 + N144 * 0.380788 + N144^2 * 1.91876$$

$$N144 = -0.00204878 + N167 * 0.382578 + N167 * N202 * 0.647188 + N202 * 0.626817 - N202^2 * 0.655717$$

$$N202 = -0.044274 - N249 * 27.4437 - N249 * N247 * 80.0187 + N249^2 * 80.0501 + N247 * 28.5628$$

$$N247 = 0.00621484 + N249 * 0.963485 + N348^2 * 0.0481015$$

$$N31 = 0.00441769 + N226 * 0.364219 - N226 * N52 * 12.9012 + N226^2 * 6.05236 + N52 * 0.610084 + N52^2 * 6.87458$$

$$N52 = -0.0646652 + N363 * 0.201776 - N363 * N74 * 0.270059 + N74 * 1.08277$$

$$N74 = -0.000760788 + N132 * 1.00215 - N132^2 * 0.40679 + N187^2 * 0.407217$$

$$N187 = 0.00418657 - N207 * 0.516945 - N207 * N240 * 125.356 + N207^2 * 65.7687 + N240 * 1.48596 + N240^2 * 59.6245$$

$$N240 = 0.0125984 + N245 * 1.84031 + N245 * N300 * 2.21798 - N245^2 * 2.14763 - N300 * 0.901969$$

$$N300 = -0.162121 + N343 * 0.838859 + N343 * N371 * 0.94242 - N343^2 * 0.227397 + N371 * 0.624239 - N371^2 * 0.638309$$

$$N226 = 0.0234405 + N245 * 2.88634 + N245 * N289 * 5.00976 - N245^2 * 4.87702 - N289 * 2.00173$$

$$N289 = -0.145798 + N348 * 0.925865 + N348 * N371 * 0.674947 - N348^2 * 0.222066 + N371 * 0.360132$$

$$N59 = 0.00762732 + N204 * 0.956563 - N204 * N77 * 8.63878 + N204^2 * 3.34262 + N77^2 * 5.34632$$

$$N77 = -0.0184702 + N139 * 1.08486 - N139 * N349 * 0.895069 + N139^2 * 0.312548 + N349^2 * 0.472899$$

$$N349 = -0.24874 + N350^2 * 1.28051 + N354 * 2.17015 - N354^2 * 2.53189$$

$$N354 = 0.542463 + N360 * 2.65141 + N360 * N365 * 11.6912 - N360^2 * 8.42761 - N365 * 4.35281$$

$$N365 = 1.33214 + x_2 * 0.0149331 - x_2 * N370 * 0.0333006 - {x_2}^2 * 4.34831 * 10^{-5} - N370 * 7.62649 + N370^2 * 13.0534$$

$$N360 = 0.768367 + x_4 * 0.0249707 - x_4 * N369 * 0.0607055 - {x_4}^2 * 7.14588 * 10^{-5} - N369 * 6.01 + N369^2 * 13.3676$$

$$N350 = 0.266342 - N363 * N366 * 34.3697 + N363^2 * 17.0505 + N366^2 * 17.6918$$

$$N366 = 2.54124 - x_2 * N371 * 0.0147577 + {x_2}^2 * 5.02424 * 10^{-5} - N371 * 14.3422 + N371^2 * 23.8769$$

$$N371 = 0.315366 + x_3 * 0.0469567 - {x_3}^2 * 0.00657724 - {x_4}^2 * 1.9964 * 10^{-5}$$

$$N363 = 3.3063 - N369 * 9.4594 + N369 * N370 * 16.3706 + N369^2 * 6.88907 - N370 * 8.43063 + N370^2 * 3.48156$$

$$N370 = 0.559466 - x_2 * 0.00928795 + x_2 * x_4 * 7.29825 * 10^{-5} + {x_2}^2 * 6.86844 * 10^{-5} - {x_4}^2 * 5.50523 * 10^{-5}$$

$$N139 = 0.0599519 - x_4 * 0.000668139 + x_4 * N198 * 0.00599168 - {x_4}^2 * 8.77286 * 10^{-6} + N198 * 0.604476 + N198^2 * 0.298508$$

$$N198 = -0.00739919 + x_1 * 1.15248 - x_1 * N227 * 3.26148 + N227^2 * 2.90253$$

$$N73 = -0.000752215 + N132 * 1.00207 - N132 * N188 * 0.80864 + N188^2 * 0.808737$$

$$N188 = 0.00842781 - N207 * N239 * 214.111 + N207^2 * 109.179 + N239 * 0.946987 + N239^2 * 104.983$$

$$N239 = -0.0283368 + N245 * 1.11063 - N245 * N357 * 0.350962 + N357^2 * 0.273286$$

$$N357 = 5.46278 - x_2 * 0.0177107 + x_2 * N369 * 0.0722021 - {x_2}^2 * 6.09357 * 10^{-5} - N369 * 30.525 + N369^2 * 43.7799$$

$$N245 = 0.00469092 + N249 * 0.986125 + N249 * N343 * 7.24005 - N249^2 * 3.63278 - N343^2 * 3.58576$$

$$N207 = 0.0117824 + N219 * 1.38854 + N219 * N339 * 9.20926 - N219^2 * 5.16005 - N339 * 0.440334 - N339^2 * 3.97121$$

$$N339 = -0.0136465 + x_4 * 0.000312714 + N343 * 1.00594$$

$$N219 = 0.000436997 + x_1 * 1.09273 - x_1 * N249 * 3.18891 + N249^2 * 2.91325$$

$$N132 = 0.0101058 + x_1 * 0.935141 - x_1 * N167 * 5.3548 + {x_1}^2 * 1.51369 + N167 * 0.092853 + N167^2 * 3.68007$$

$$N167 = -0.0234471 + x_2 * 0.00133983 - x_2 * N201 * 0.000893987 - {x_2}^2 * 1.84993 * 10^{-5} + N201 * 1.05634 - N201^2 * 0.0308196$$

$$N153 = 0.00644219 + N183 * 0.467566 - N183 * N204 * 36.2981 + N183^2 * 18.1295 + N204 * 0.49205 + N204^2 * 18.2057$$

$$N204 = -0.0027637 + N227 * 1.56905 + N227 * N298 * 29.99 - N227^2 * 15.4078 - N298 * 0.517987 - N298^2 * 14.6533$$

$$N298 = -0.213135 + x_1 * 1.5415 - {x_1}^2 * 0.716435 + N369 * 0.529644$$

$$N369 = 0.424808 - x_2 * 0.00602004 + x_2 * x_3 * 8.13487 * 10^{-5} + {x_2}^2 * 5.75127 * 10^{-5} + x_3 * 0.0422081 - {x_3}^2 * 0.0066477$$

$$N227 = -0.00118403 + x_3 * 0.0168248 + N343 * 0.794964 + N343^2 * 0.266735$$

$$N343 = -0.0165124 + x_1 * 1.5302 - {x_1}^2 * 0.674759 - x_2 * 0.000460021$$

$$N183 = 0.000386682 - N201 * 0.644518 - N201 * N222 * 109.562 + N201^2 * 56.6588 + N222 * 1.62812 + N222^2 * 52.925$$

$$N222 = -0.00215233 + x_3 * 0.0172009 + N348 * 0.794615 + N348^2 * 0.268923$$

$$N348 = -0.0241623 + x_1 * 1.39918 + x_1 * x_4 * 0.00120499 - {x_1}^2 * 0.521387$$

$$N201 = 0.0833688 - x_4 * 0.00161256 + x_4 * N249 * 0.00682585 + N249 * 0.555885 + N249^2 * 0.332771$$

$$N249 = -0.0483794 + x_1 * 1.37161 - {x_1}^2 * 0.430654 + x_3 * 0.01662$$

References

1. Gan, Y.Y.; Ong, H.C.; Ling, T.C.; Zulkifli, N.W.M.; Wang, C.T.; Yang, Y.C. Thermal conductivity optimization and entropy generation analysis of titanium dioxide nanofluid in evacuated tube solar collector. *Appl. Therm. Eng.* **2018**, *145*, 155–164. [CrossRef]
2. Jedi, A.; Razali, N.; Wan Mahmood, W.M.F.; Bakar, N.A.A. Statistical Criteria of Nanofluid Flows over a Stretching Sheet with the Effects of Magnetic Field and Viscous Dissipation. *Symmetry* **2019**, *11*, 1367. [CrossRef]
3. Safaei, M.R.; Togun, H.; Vafai, K.; Kazi, S.N.; Badarudin, A. Investigation of Heat Transfer Enhancement in a Forward-Facing Contracting Channel Using FMWCNT Nanofluids. *Numer. Heat Transf. Part A Appl.* **2014**, *66*, 1321–1340. [CrossRef]
4. Rafique, K.; Anwar, M.I.; Misiran, M.; Khan, I.; Seikh, A.H.; Sherif, E.-S.M.; Nisar, K.S. Numerical Analysis with Keller-Box Scheme for Stagnation Point Effect on Flow of Micropolar Nanofluid over an Inclined Surface. *Symmetry* **2019**, *11*, 1379. [CrossRef]
5. Esfe, M.H.; Rejvani, M.; Karimpour, R.; Abbasian Arani, A.A. Estimation of thermal conductivity of ethylene glycol-based nanofluid with hybrid suspensions of SWCNT–Al_2O_3 nanoparticles by correlation and ANN methods using experimental data. *J. Therm. Anal. Calorim.* **2017**, *128*, 1359–1371. [CrossRef]
6. Arani, A.A.A.; Akbari, O.A.; Safaei, M.R.; Marzban, A.; Alrashed, A.A.A.A.; Ahmadi, G.R.; Nguyen, T.K. Heat transfer improvement of water/single-wall carbon nanotubes (SWCNT) nanofluid in a novel design of a truncated double-layered microchannel heat sink. *Int. J. Heat Mass Transf.* **2017**, *113*, 780–795. [CrossRef]
7. Albojamal, A.; Hamzah, H.; Haghighi, A.; Vafai, K. Analysis of nanofluid transport through a wavy channel. *Numer. Heat Transf. Part A Appl.* **2017**, *72*, 869–890. [CrossRef]
8. Irandoost Shahrestani, M.; Maleki, A.; Safdari Shadloo, M.; Tlili, I. Numerical Investigation of Forced Convective Heat Transfer and Performance Evaluation Criterion of Al_2O_3/Water Nanofluid Flow inside an Axisymmetric Microchannel. *Symmetry* **2020**, *12*, 120. [CrossRef]
9. Shamaeil, M.; Firouzi, M.; Fakhar, A. The effects of temperature and volume fraction on the thermal conductivity of functionalized DWCNTs/ethylene glycol nanofluid. *J. Therm. Anal. Calorim.* **2016**, *126*, 1455–1462. [CrossRef]
10. Guo, W.; Li, G.; Zheng, Y.; Dong, C. Measurement of the thermal conductivity of SiO_2 nanofluids with an optimized transient hot wire method. *Thermochim. Acta* **2018**, *661*, 84–97. [CrossRef]
11. Agarwal, R.; Verma, K.; Agrawal, N.K.; Singh, R. Sensitivity of thermal conductivity for Al_2O_3 nanofluids. *Exp. Therm. Fluid Sci.* **2017**, *80*, 19–26. [CrossRef]
12. Bagheri, H.; Ahmadi Nadooshan, A. The effects of hybrid nano-powder of zinc oxide and multi walled carbon nanotubes on the thermal conductivity of an antifreeze. *Phys. E Low-Dimens. Syst. Nanostructures* **2018**, *103*, 361–366. [CrossRef]
13. Abbasi, F.M.; Gul, M.; Shehzad, S.A. Hall effects on peristalsis of boron nitride-ethylene glycol nanofluid with temperature dependent thermal conductivity. *Phys. E Low-Dimens. Syst. Nanostructures* **2018**, *99*, 275–284. [CrossRef]
14. Jiang, H.; Zhang, Q.; Shi, L. Effective thermal conductivity of carbon nanotube-based nanofluid. *J. Taiwan Inst. Chem. Eng.* **2015**, *55*, 76–81. [CrossRef]

15. Kumar, M.S.; Vasu, V.; Gopal, A.V. Thermal conductivity and rheological studies for Cu–Zn hybrid nanofluids with various basefluids. *J. Taiwan Inst. Chem. Eng.* **2016**, *66*, 321–327. [CrossRef]
16. Ahmadi, M.H.; Mirlohi, A.; Alhuyi Nazari, M.; Ghasempour, R. A review of thermal conductivity of various nanofluids. *J. Mol. Liq.* **2018**, *265*, 181–188. [CrossRef]
17. Hemmat Esfe, M.; Abbasian Arani, A.A.; Shafiei Badi, R.; Rejvani, M. ANN modeling, cost performance and sensitivity analyzing of thermal conductivity of DWCNT–SiO_2/EG hybrid nanofluid for higher heat transfer. *J. Therm. Anal. Calorim.* **2018**, *131*, 2381–2393. [CrossRef]
18. Reddy, K.S.; Kamnapure, N.R.; Srivastava, S. Nanofluid and nanocomposite applications in solar energy conversion systems for performance enhancement: A review. *Int. J. Low-Carbon Technol.* **2016**, *12*, ctw007. [CrossRef]
19. Gandomkar, A.; Saidi, M.H.; Shafii, M.B.; Vandadi, M.; Kalan, K. Visualization and comparative investigations of pulsating Ferro-fluid heat. *Appl. Therm. Eng.* **2017**, *116*, 56–65. [CrossRef]
20. Leong, K.Y.; Saidur, R.; Mahlia, T.M.I.; Yau, Y.H. Performance investigation of nanofluids as working fluid in a thermosyphon air preheater. *Int. Commun. Heat Mass Transf.* **2012**, *39*, 523–529. [CrossRef]
21. Ahmadi, M.H.; Ramezanizadeh, M.; Nazari, M.A.; Lorenzini, G.; Kumar, R.; Jilte, R. Applications of nanofluids in geothermal: A review. *Math. Model. Eng. Probl.* **2018**, *5*, 281–285. [CrossRef]
22. Akbari, O.A.; Safaei, M.R.; Goodarzi, M.; Akbar, N.S.; Zarringhalam, M.; Shabani, G.A.S.; Dahari, M. A modified two-phase mixture model of nanofluid flow and heat transfer in a 3-D curved microtube. *Adv. Powder Technol.* **2016**, *27*, 2175–2185. [CrossRef]
23. Behnampour, A.; Akbari, O.A.; Safaei, M.R.; Ghavami, M.; Marzban, A.; Sheikh Shabani, G.A.; Zarringhalam, M.; Mashayekhi, R. Analysis of heat transfer and nanofluid fluid flow in microchannels with trapezoidal, rectangular and triangular shaped ribs. *Phys. E Low-Dimens. Syst. Nanostructures* **2017**, *91*, 15–31. [CrossRef]
24. Abdollahzadeh Jamalabadi, M.; Ghasemi, M.; Alamian, R.; Wongwises, S.; Afrand, M.; Shadloo, M. Modeling of Subcooled Flow Boiling with Nanoparticles under the Influence of a Magnetic Field. *Symmetry* **2019**, *11*, 1275. [CrossRef]
25. Elsayed, A.; Al-dadah, R.K.; Mahmoud, S.; Rezk, A. Numerical investigation of turbulent flow heat transfer and pressure drop of AL_2O_3/water nanofluid in helically coiled tubes. *Int. J. Low-Carbon Technol.* **2015**, *10*, 275–282. [CrossRef]
26. Karana, D.R.; Sahoo, R.R. Effect on TEG performance for waste heat recovery of automobiles using MgO and ZnO nanofluid coolants. *Case Stud. Therm. Eng.* **2018**, *12*, 358–364. [CrossRef]
27. Asadi, A.; Pourfattah, F. Heat transfer performance of two oil-based nanofluids containing ZnO and MgO nanoparticles; a comparative experimental investigation. *Powder Technol.* **2019**, *343*, 296–308. [CrossRef]
28. Verma, S.K.; Tiwari, A.K.; Chauhan, D.S. Performance augmentation in flat plate solar collector using MgO/water nanofluid. *Energy Convers. Manag.* **2016**, *124*, 607–617. [CrossRef]
29. Menlik, T.; Sözen, A.; Gürü, M.; Öztaş, S. Heat transfer enhancement using MgO/water nanofluid in heat pipe. *J. Energy Inst.* **2015**, *88*, 247–257. [CrossRef]
30. Toghraie, D.; Sina, N.; Jolfaei, N.A.; Hajian, M.; Afrand, M. Designing an Artificial Neural Network (ANN) to predict the viscosity of Silver/Ethylene glycol nanofluid at different temperatures and volume fraction of nanoparticles. *Phys. A Stat. Mech. Its Appl.* **2019**, *534*, 122142. [CrossRef]
31. Hemmat Esfe, M. Mathematical and artificial brain structure-based modeling of heat conductivity of water based nanofluid enriched by double wall carbon nanotubes. *Phys. A Stat. Mech. Its Appl.* **2019**, *540*, 120766. [CrossRef]
32. Saeedi, A.H.; Akbari, M.; Toghraie, D. An experimental study on rheological behavior of a nanofluid containing oxide nanoparticle and proposing a new correlation. *Phys. E Low-Dimens. Syst. Nanostructures* **2018**, *99*, 285–293. [CrossRef]
33. Ahmadi, M.-A.; Ahmadi, M.H.; Fahim Alavi, M.; Nazemzadegan, M.R.; Ghasempour, R.; Shamshirband, S. Determination of thermal conductivity ratio of CuO/ethylene glycol nanofluid by connectionist approach. *J. Taiwan Inst. Chem. Eng.* **2018**, *91*, 383–395. [CrossRef]
34. Safaei, M.R.; Hajizadeh, A.; Afrand, M.; Qi, C.; Yarmand, H.; Zulkifli, N.W.B.M. Evaluating the effect of temperature and concentration on the thermal conductivity of ZnO-TiO_2/EG hybrid nanofluid using artificial neural network and curve fitting on experimental data. *Phys. A Stat. Mech. Its Appl.* **2019**, *519*, 209–216. [CrossRef]

35. Bagherzadeh, S.A.; D'Orazio, A.; Karimipour, A.; Goodarzi, M.; Bach, Q.-V. A novel sensitivity analysis model of EANN for F-MWCNTs–Fe_3O_4/EG nanofluid thermal conductivity: Outputs predicted analytically instead of numerically to more accuracy and less costs. *Phys. A Stat. Mech. Its Appl.* **2019**, *521*, 406–415. [CrossRef]
36. Alnaqi, A.A.; Sayyad Tavoos Hal, S.; Aghaei, A.; Soltanimehr, M.; Afrand, M.; Nguyen, T.K. Predicting the effect of functionalized multi-walled carbon nanotubes on thermal performance factor of water under various Reynolds number using artificial neural network. *Phys. A Stat. Mech. Its Appl.* **2019**, *521*, 493–500. [CrossRef]
37. Komeilibirjandi, A.; Hossein, A.; Akbar, R. Thermal conductivity prediction of nanofluids containing CuO nanoparticles by using correlation and artificial neural network. *J. Therm. Anal. Calorim.* **2019**. [CrossRef]
38. Wu, H.; Al-Rashed, A.A.A.A.; Shahsavar, A.; Karimi, A.; Sardari, P.T. Curve-fitting on experimental thermal conductivity of motor oil under influence of hybrid nano additives containing multi-walled carbon nanotubes and zinc oxide. *Phys. A Stat. Mech. Its Appl.* **2019**, *535*, 122128. [CrossRef]
39. Ramezanizadeh, M.; Alhuyi Nazari, M.; Ahmadi, M.H.; Lorenzini, G.; Pop, I. A review on the applications of intelligence methods in predicting thermal conductivity of nanofluids. *J. Therm. Anal. Calorim.* **2019**, 1–17. [CrossRef]
40. Ahmadi, M.H.; Alhuyi Nazari, M.; Ghasempour, R.; Madah, H.; Shafii, M.B.; Ahmadi, M.A. Thermal conductivity ratio prediction of Al_2O_3/water nanofluid by applying connectionist methods. *Colloids Surf. A Physicochem. Eng. Asp.* **2018**, *541*, 154–164. [CrossRef]
41. Ahmadi, M.H.; Ahmadi, M.A.; Nazari, M.A.; Mahian, O.; Ghasempour, R. A proposed model to predict thermal conductivity ratio of Al_2O_3/EG nanofluid by applying least squares support vector machine (LSSVM) and genetic algorithm as a connectionist approach. *J. Therm. Anal. Calorim.* **2019**, *135*, 271–281. [CrossRef]
42. Ahmadi, M.H.; Baghban, A.; Sadeghzadeh, M.; Hadipoor, M.; Ghazvini, M. Evolving connectionist approaches to compute thermal conductivity of TiO_2/water nanofluid. *Phys. A Stat. Mech. Its Appl.* **2019**, *540*, 122489. [CrossRef]
43. Oduro, S.D.; Metia, S.; Duc, H.; Ha, Q.P. Predicting Carbon Monoxide Emissions with Multivariate Adaptive Regression Splines (MARS) and Artificial Neural Networks (ANNs). In Proceedings of the 32nd International Symposium on Automation and Robotics in Construction and Mining (ISARC 2015), Oulu, Finland, 15–18 June 2015.
44. Put, R.; Xu, Q.S.; Massart, D.L.; Vander Heyden, Y. Multivariate adaptive regression splines (MARS) in chromatographic quantitative structure-retention relationship studies. *J. Chromatogr. A* **2004**, *1055*, 11–19. [CrossRef] [PubMed]
45. Xu, Q.-S.; Daszykowski, M.; Walczak, B.; Daeyaert, F.; de Jonge, M.R.; Heeres, J.; Koymans, L.M.H.; Lewi, P.J.; Vinkers, H.M.; Janssen, P.A.; et al. Multivariate adaptive regression splines—Studies of HIV reverse transcriptase inhibitors. *Chemom. Intell. Lab. Syst.* **2004**, *72*, 27–34. [CrossRef]
46. Rounaghi, M.M.; Abbaszadeh, M.R.; Arashi, M. Stock price forecasting for companies listed on Tehran stock exchange using multivariate adaptive regression splines model and semi-parametric splines technique. *Phys. A Stat. Mech. Its Appl.* **2015**, *438*, 625–633. [CrossRef]
47. Chao, K.-W.; Hu, N.-Z.; Chao, Y.-C.; Su, C.-K.; Chiu, W.-H. Implementation of Artificial Intelligence for Classification of Frogs in Bioacoustics. *Symmetry* **2019**, *11*, 1454. [CrossRef]
48. Islam, K.T.; Raj, R.G.; Mujtaba, G. Recognition of Traffic Sign Based on Bag-of-Words and Artificial Neural Network. *Symmetry* **2017**, *9*, 138. [CrossRef]
49. Yazdani-Chamzini, A.; Zavadskas, E.; Antucheviciene, J.; Bausys, R. A Model for Shovel Capital Cost Estimation, Using a Hybrid Model of Multivariate Regression and Neural Networks. *Symmetry* **2017**, *9*, 298. [CrossRef]
50. Gholipour Khajeh, M.; Maleki, A.; Rosen, M.A.; Ahmadi, M.H. Electricity price forecasting using neural networks with an improved iterative training algorithm. *Int. J. Ambient Energy* **2018**, *39*, 147–158. [CrossRef]
51. Zhang, W.; Maleki, A.; Rosen, M.A. A heuristic-based approach for optimizing a small independent solar and wind hybrid power scheme incorporating load forecasting. *J. Clean. Prod.* **2019**, *241*, 117920. [CrossRef]
52. Ramezanizadeh, M.; Ahmadi, M.H.; Nazari, M.A.; Sadeghzadeh, M.; Chen, L. A review on the utilized machine learning approaches for modeling the dynamic viscosity of nanofluids. *Renew. Sustain. Energy Rev.* **2019**, *114*, 109345. [CrossRef]

53. Mohamadian, F.; Eftekhar, L.; Haghighi Bardineh, Y. Applying GMDH artificial neural network to predict dynamic viscosity of an antimicrobial nanofluid. *Mashhad Univ. Med. Sci.* **2018**, *5*, 217–221.
54. Pourkiaei, S.M.; Ahmadi, M.H.; Hasheminejad, S.M. Modeling and experimental verification of a 25W fabricated PEM fuel cell by parametric and GMDH-type neural network. *Mech. Ind.* **2016**, *17*, 105. [CrossRef]
55. Jiang, Y.; Sulgani, M.T.; Ranjbarzadeh, R.; Karimipour, A.; Nguyen, T.K. Hybrid GMDH-type neural network to predict fluid surface tension, shear stress, dynamic viscosity & sensitivity analysis based on empirical data of iron(II) oxide nanoparticles in light crude oil mixture. *Phys. A Stat. Mech. Its Appl.* **2019**, *526*, 120948.
56. Hemmat Esfe, M.; Afrand, M.; Karimipour, A.; Yan, W.-M.; Sina, N. An experimental study on thermal conductivity of MgO nanoparticles suspended in a binary mixture of water and ethylene glycol. *Int. Commun. Heat Mass Transf.* **2015**, *67*, 173–175. [CrossRef]
57. Kim, S.H.; Choi, S.R.; Kim, D. Thermal Conductivity of Metal-Oxide Nanofluids: Particle Size Dependence and Effect of Laser Irradiation. *J. Heat Transf.* **2007**, *129*, 298. [CrossRef]
58. Żyła, G. Viscosity and thermal conductivity of MgO–EG nanofluids. *J. Therm. Anal. Calorim.* **2017**, *129*, 171–180. [CrossRef]
59. Xie, H.; Yu, W.; Chen, W. MgO nanofluids: Higher thermal conductivity and lower viscosity among ethylene glycol-based nanofluids containing oxide nanoparticles. *J. Exp. Nanosci.* **2010**, *5*, 463–472. [CrossRef]
60. Hemmat Esfe, M.; Saedodin, S.; Bahiraei, M.; Toghraie, D.; Mahian, O.; Wongwises, S. Thermal conductivity modeling of MgO/EG nanofluids using experimental data and artificial neural network. *J. Therm. Anal. Calorim.* **2014**, *118*, 287–294. [CrossRef]